# Nonlinear Reduced-Order Simulation Using Stress-Free and Pre-Stressed Modal Bases

Adam Przekop[1]
*Analytical Services and Materials, Inc., Hampton, VA, 23666*

Michael A. Stover[2]
*Virginia Tech, Blacksburg, VA, 24061*

*and*

Stephen A. Rizzi[3]
*NASA Langley Research Center, Hampton, VA, 23681*

**A study is undertaken to determine the advantages and disadvantages associated with application of stress-free and pre-stressed modal bases in a reduced-order finite-element-based nonlinear simulation. A planar beam is chosen as an application example and its response due to combined thermal and random pressure loadings is examined. Combinations of two random pressure levels and two thermal conditions are investigated. The latter consists of an ambient temperature condition and an elevated temperature condition in the post-buckled regime. It is found that stress-free normal modes establish a broadly applicable modal basis yielding accurate results for all the loading regimes considered. In contrast, the range of applicability for a thermally pre-stressed modal basis is found to be limited. The behavior is explained by scrutinizing the coupling found in the linear stiffness and the effect this coupling has on the structural response characteristics under the range of loading conditions considered.**

## Nomenclature

| | | |
|---|---|---|
| $a$ | = | quadratic modal stiffness coefficient |
| $b$ | = | cubic modal stiffness coefficient |
| $[C],[\tilde{C}]$ | = | physical degree-of-freedom damping matrix, modal damping matrix |
| $d$ | = | linear modal stiffness coefficient |
| $\Delta T$ | = | temperature increment |
| $\{f\},\{\tilde{f}\}$ | = | physical degree-of-freedom force vector, modal force vector |
| $\{f_{NL}\},\{\tilde{f}_{NL}\}$ | = | nonlinear physical degree-of-freedom restoring force vector, nonlinear modal restoring force vector |
| $[\Phi],\{\varphi\}$ | = | matrix of normal modes, normal mode vector |
| $[I]$ | = | identity matrix |
| $L$ | = | number of modal basis functions |
| $[\lambda]$ | = | proper orthogonal value matrix |
| $m$ | = | number of nodes in finite element model |
| $M$ | = | number of most contributing proper orthogonal modes |
| $[M],[\tilde{M}]$ | = | physical degree-of-freedom mass matrix, modal mass matrix |
| $n$ | = | number of displacement fields used in snapshot matrix |

[1] Senior Structural Engineer, AIAA Senior Member
[2] Graduate Student, Department of Mechanical Engineering, Randolph Hall, ASME Member
[3] Senior Research Engineer, Structural Acoustics Branch, AIAA Associate Fellow

| | | |
|---|---|---|
| $N$ | = | number of physical degrees-of-freedom |
| $[P], \{p\}$ | = | matrix of proper orthogonal modes, proper orthogonal mode vector |
| $q$ | = | modal (generalized) coordinate |
| $[R]$ | = | correlation matrix |
| $t$ | = | time |
| $u$ | = | in-plane displacement component |
| $\upsilon$ | = | cumulative proper orthogonal mode participation factor |
| $w$ | = | transverse displacement component |
| $[X], \{x\}$ | = | displacement snapshot matrix, displacement time history vector |
| $\chi_i$ | = | $i^{th}$ proper orthogonal mode participation factor |
| $\zeta$ | = | viscous damping factor |
| $\psi$ | = | rotational component |
| $\omega$ | = | undamped natural frequency |

## I. Introduction

HIGH-PERFORMANCE aerospace vehicle structures are subjected to a broad range of extreme loading environments which can result in nonlinear structural response.[1] Commercial-off-the-shelf finite element (FE) tools are capable of analyzing such response regimes, but do so at a computational expense that is often deemed prohibitive. Consequently, a more computationally efficient reduced-order nonlinear simulation is sought. A critical step in forming an accurate and robust reduced-order system is the selection of a modal basis. Until recently, the process of selecting the modal basis was often quite arbitrary, and relied heavily on a subjective judgment of the analyst.

The authors recently offered a procedure through which an accurate and efficient modal basis selection can be accomplished.[2-4] The procedure is based on system identification via Proper Orthogonal Decomposition (POD).[5,6] The POD analysis is typically performed under the most severe loading condition expected such that all of the relevant nonlinear dynamics are captured. Once the Proper Orthogonal Modes (POMs) are determined by the POD, they are used to guide a selection of similar normal modes through application of either a modal expansion[2] (ME) or a modal assurance criterion[7] (MAC) approach. The above procedure has been shown to be very useful in guiding a modal basis selection within a particular class of basis functions, e.g. stress-free modes. However, the procedure does not address the question of which class of basis functions is preferred. Here, the meaning of a preferred basis is one in which a fewer number of modes, relative to a larger basis, offer comparably accurate results. The present study aims to investigate this issue by examining a problem in which a random acoustic loading combined with quasi-steady thermal loading is present, giving two relevant classes of basis functions, i.e. stress-free and thermally pre-stressed normal modes.

Several researchers in the past have investigated the application of pre-stressed modal bases. Guo and Mei[8] used the so-called aero-elastic modes to solve a panel flutter problem. Guo et al.[9] investigated pre-stressed modes in the context of a thermal buckling suppression control problem using shape memory alloys. Spottswood et al.[10] examined thermally pre-stressed normal modes applied to shallowly curved structures. While most researchers concluded that advantages of the pre-stressed bases were evident in their studies, they only addressed the loading condition under which the basis was obtained. In many practical engineering applications, however, the loading conditions change drastically over the mission cycle and therefore there exists a strong incentive to apply a single modal basis to the analysis of a broad range of loading regimes. This work attempts to address some of the aspects of the application of the stress-free and pre-stressed bases to a range of loading conditions, so that a single robust reduced-order system can be formed that is applicable to multiple loading scenarios.

## II. Formulation

The system identification employed by the authors[2,4] is next reviewed and the modal basis selection criterion employing the MAC approach[7] is summarized. The previously developed modal system reduction by an indirect nonlinear stiffness evaluation procedure,[11,12] referred to as RANSTEP for Reduced-order Analysis using a Nonlinear STiffness Evaluation Procedure, is also briefly discussed.

### A. System Identification – Proper Orthogonal Decomposition

When physical degrees-of-freedom (DoFs) are chosen to characterize the response, a snapshot matrix $[X]$ can be formed as an accumulation of $n$ instantaneous displacement, velocity, or acceleration response fields.[5,6] In the current analysis, displacement fields obtained from a full-order nonlinear FE analysis are used, resulting in a snapshot matrix of size $n \times N$, where $N$ is the number of DoFs. The sample rate and spatial resolution of the snapshot matrix must be sufficient to resolve the system's temporal and spatial characteristics of interest. The correlation matrix $[R]$, of size $N \times N$, is formed as

$$[R] = \frac{1}{n}[X]^T [X]. \tag{1}$$

An eigenanalysis of the correlation matrix is next performed, i.e,

$$\left([R] - [\lambda][I]\right)\{p\} = \{0\} \tag{2}$$

to obtain the POM matrix $[P] = \left[\{p_1\}\{p_2\}\ldots\{p_N\}\right]$ and the diagonal proper orthogonal value (POV) matrix, $[\lambda]$, both of size $N \times N$. Each POV is a measure of the corresponding POM activity, i.e., the higher the POV, the greater the contribution of a corresponding POM to the dynamic response.

The POD procedure employed is performed independently for each DoF type of interest by partitioning the snapshot matrix. In the subsequent POD analyses, two out of three available DoF types for single-plane bending beam FEs are considered, namely, the transverse ($w$) and in-plane displacement ($u$) components. The rotational component ($\psi_y$) was previously found[2] to ultimately yield the same set of normal modes (NMs) as the transverse displacement DoF, so it is not considered in the present analysis. By adopting this approach, the size of each individual DoF snapshot matrix $[X]$ is reduced to $n \times m$, where $m$ is the number of nodes, and the size of each individual correlation matrix $[R]$, POM matrix $[P]$, and POV matrix $[\lambda]$ is reduced to $m \times m$.

### B. Modal Basis Selection

The contribution of each POM to the overall dynamic response is given by

$$\chi_i = \lambda_i \Big/ \sum_{j=1}^{m} \lambda_j \qquad i = 1, \ldots, m \tag{3}$$

where $\chi_i$ is the $i^{th}$ POM participation factor. The sum of all POM participation factors is unity. When the most contributing $M$ POMs are selected, their cumulative participation, $\upsilon$, can be expressed as

$$\upsilon = \sum_{i=1}^{M} \chi_i \qquad 0 < \upsilon \le 1 \ . \tag{4}$$

Retention of only the selected $M$ POMs further reduces the size of $[P]$ to $m$ x $M$.

Next, a set of NMs which either directly resemble, or can be superposed to resemble the POMs can be sought. The authors recently presented two criteria for identifying such a set using the MAC[2,4] and the ME approaches.[2,3] Based on the previous studies, it was concluded the MAC approach is generally more applicable to cases where POMs and NMs are well correlated, while the ME approach is better suited for use when the POMs bear little direct resemblance to NMs. Since the POMs and NMs considered in this study are well correlated, the MAC approach is used herein.

*Modal Assurance Criterion Approach*

A measure of similarity of two vectors, e.g. a POM vector $\{p_k\}$ and the normal mode vector $\{\varphi_l\}$ may be quantified by the scalar MAC value[7]

$$MAC\left(\{p_k\},\{\varphi_l\}\right) = \frac{\left|\{p_k\}^T \{\varphi_l\}\right|^2}{\left(\{p_k\}^T \{p_k\}\right)\left(\{\varphi_l\}^T \{\varphi_l\}\right)}. \tag{5}$$

The MAC assumes values from 0 to 1, where a value of 0 signifies the vectors are completely uncorrelated and a value of 1 indicates a perfect shape match. The relative amplitudes of the two vectors do not affect the MAC values. In FE analysis/test model verification work, a MAC value above 0.8-0.9 is often used for target modes. Since the linear NMs are not expected to be the same as the POMs, which may be derived from a strongly nonlinear response analysis, a less stringent requirement for a MAC value above 0.5 is assumed in the present study. Thus, for the selected POMs, normal modes with MAC values of 0.5 or greater are included in the reduced-order analysis. Unlike the POD/ME approach where at least one NM will always be identified for each POM, the POD/MAC approach will not do so when the MAC is below the threshold.

### C. Nonlinear Reduced-Order Analysis

Once a set of basis functions consisting of NMs is selected using the MAC, the nonlinear modal reduction of the system can proceed. A reduced-order method gains its computational advantage by reducing the size of the system in physical DoFs (full-order) to a much smaller system expressed in generalized coordinates (reduced-order). For the problem of interest, the equation of motion in physical DoFs is expressed as

$$[M]\{\ddot{x}(t)\}+[C]\{\dot{x}(t)\}+\{f_{NL}(x(t),\Delta T)\}=\{f(t)\}, \tag{6}$$

where $[M]$ and $[C]$ are the structural mass and damping matrices, and $\{x\}$, $\{f_{NL}\}$, and $\{f\}$ are the physical displacement, nonlinear restoring force, and excitation force vectors, respectively. By applying the modal transformation

$$\{x(t)\}=[\Phi]\{q(t)\}, \tag{7}$$

the equation of motion is expressed in reduced-order form as

$$\left[\tilde{M}\right]\{\ddot{q}(t)\}+\left[\tilde{C}\right]\{\dot{q}(t)\}+\{\tilde{f}_{NL}(q_1(t),q_1(t),\ldots,q_L(t),\Delta T)\}=\{\tilde{f}(t)\} \tag{8}$$

where $\{q\}$ is a generalized coordinate vector and $[\Phi]$ is a matrix containing $L$ selected NMs of the basis. The modal nonlinear restoring force in Eq. (8) is obtained by

$$\{\tilde{f}_{NL}\}=[\Phi]^T\{f_{NL}\}\ . \tag{9}$$

Because mass-normalized NMs are used as the basis functions, the modal mass and damping matrices can be expressed as

$$\left[\tilde{M}\right]=[\Phi]^T[M][\Phi]=\lceil I\rfloor \qquad \left[\tilde{C}\right]=[\Phi]^T[C][\Phi]=\lceil 2\zeta_r\omega_r\rfloor, \tag{10}$$

where $\omega_r$ and $\zeta_r$ are the undamped natural frequencies and the viscous damping factors, respectively. The modal excitation force vector is given by $\{\tilde{f}(t)\}=[\Phi]^T\{f(t)\}$.

The system reduction utilized in this study is based on the indirect approach employing a nonlinear stiffness evaluation procedure.[11,12] In general the procedure expresses the $r^{\text{th}}$ component of the nonlinear modal restoring force vector as

$$\tilde{f}^r_{\mathrm{NL}}(q_1,\ldots,q_L,\Delta T)=\sum_{j=1}^{L}d^r_j(\Delta T)q_j+\sum_{j=1}^{L}\sum_{k=j}^{L}a^r_{jk}(\Delta T)q_jq_k+\sum_{j=1}^{L}\sum_{k=j}^{L}\sum_{l=k}^{L}b^r_{jkl}(\Delta T)q_jq_kq_l \qquad r=1,\ldots,L \tag{11}$$

where $d$, $a$, and $b$ are the linear, quadratic, and cubic modal stiffness coefficients. It is known, however, that for planar and isotropic structures, only linear coefficients $d$ depend on the temperature increment $\Delta T$.[13] Different combinations of scaled NMs are used to form a set of prescribed displacement fields. The normal mode vectors are scaled by the generalized coordinates $\{q\}$ to obtain physically meaningful magnitudes. Using a nonlinear static FE analysis, the nonlinear restoring forces corresponding to each prescribed displacement field under the temperature increment of interest are computed in physical DoFs and transformed to generalized coordinates per Eq. (9). As the vector $\{f_{NL}\}$ and the generalized coordinates $\{q\}$ are known, Eq. (11) constitutes a system of algebraic equations from which the linear, quadratic, and cubic modal stiffness coefficients may be determined. The number of unknown coefficients, and hence the number of nonlinear static solutions required for a transformation utilizing $L$ modes is

$$Number\ of\ \ NL\ Static\ Solutions = 3\binom{L}{1} + 3\binom{L}{2} + \binom{L}{3} \qquad L \geq 3 \tag{12}$$

where

$$\binom{L}{k} = \frac{L!}{k!(L-k)!} \ . \tag{13}$$

Note that the three terms in Eq. (12) reflect the number of linear, quadratic, and cubic modal stiffness coefficients, respectively. The number of nonlinear static solutions can be viewed as a measure of the fixed cost of the reduced-order analysis, as the modal reduction must be performed regardless of the simulated response time to be eventually computed. Once the coefficients have been determined, Eq. (8) is integrated using a fourth-order Runge-Kutta scheme and the physical displacements recovered through Eq. (7). The reduced-order analysis was implemented in the code RANSTEP,[12] which can use either the ABAQUS[14] or MSC.NASTRAN[15] FE codes for NMs analysis, nonlinear static solutions, and stress/strain recovery.

## III. Numerical Example

The following section presents results obtained using reduced-order simulations based on stress-free normal modes obtained at ambient temperature and based on pre-stressed normal modes obtained at elevated temperature. Because the linear stiffness terms are functions of temperature, their evaluation must be performed at the temperature condition analyzed, even though the particular set of normal modes used is the same.[13] In the following, two temperature conditions are analyzed. Therefore, four stiffness evaluations are performed under the following conditions; stress-free modes at ambient temperature, stress-free modes at elevated temperature, pre-stressed modes at ambient temperature, and pre-stressed modes at elevated temperature. To assess the simulation quality, the reduced-order results are compared with results obtained from a computationally intensive simulation in physical DoFs.

### A. Finite Element Model

An isotropic beam clamped at both ends served as the numerical test article. The structure under investigation, shown in Figure 1, measured 457.2 x 25.4 x 2.0 mm ($l$ x $w$ x $h$). Aluminum material properties used in the study were: Young's modulus $E$ = 73.11 GPa, Poison ratio $\nu$ = 0.325, and mass density $\rho$ = 2763 kg/m$^3$. A mass proportional damping of $C$ = 14.52 1/s was applied, which corresponded to 2.0 % critical damping at the ambient temperature fundamental frequency $f_1$ = 57.8 Hz. The thermal expansion coefficient used in the elevated temperature analysis was $\alpha = 22.32 \frac{\mu m/m}{°C}$

A single FE model of the beam was constructed for both the full-order and reduced-order analyses. It consisted of 144 ABAQUS B21 beam elements defined by 145 nodes for the total of 435 DoFs. The B21 element has two nodes, each with two translational and one rotational DoFs. All elements used had a length of 3.175 mm. The full-order nonlinear response of the beam was analyzed in physical DoFs using the ABAQUS/Explicit solution with the automatic time step selection scheme referred to in ABAQUS as "element-by-element" method.

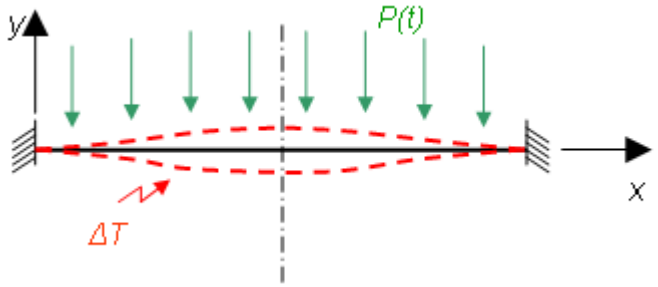


Figure 1: Beam under combined thermal and acoustic loading.

## B. Thermal-Acoustic Loading

The beam was simultaneously subjected to a uniformly distributed random pressure loading, $P(t)$, and a uniformly distributed time invariant thermal loading, $\Delta T$, having zero through-the-thickness variation. Band-limited white noise random pressure time histories were generated by summing equal amplitude random phase sine waves at a frequency resolution of 0.61 Hz in the frequency range 0 – 1500 Hz.[16] Two pressure loadings having overall sound pressure levels (OASPL) of 128 and 170 dB (re: 20 μPa) were considered.

Two thermal loading conditions were considered. An ambient temperature ($\Delta T = 0$) case served as an unstressed reference condition and the thermally post-buckled response was investigated with a temperature increment of 19.44°C (35°F), i.e., 5.3 times the critical buckling temperature of $\Delta T_{cr} = 3.67$°C (6.6°F). The post-buckled condition had two static non-zero symmetric equilibrium positions, as depicted by the red dashed line in Figure 1. For this condition, the response was previously shown[13] to evolve from small amplitude vibration around one of the post-buckled equilibrium positions (at 128 dB), to intermittent snap-through (at 158 dB), and finally to persistent snap-through between the two equilibrium positions (at 170 dB).

In the remainder of the paper, the combined load case is specified via the shorthand notation x°F/y dB, where x is the temperature increment and y is the sound pressure level.

## C. Results

Eigenanalyses of the stress-free ($\Delta T = 0$) and thermally pre-stressed beam in post-buckled regime ($\Delta T = 35$°F) are first performed to obtain the two distinct sets of normal modes from which the two distinct modal bases can be selected. The normal modes obtained under these two conditions are subsequently referred to as *cold* and *hot modes*, respectively. Next, a short response sample of the most severe loading condition under consideration, i.e., 35°F/170 dB, is simulated using physical DoFs analysis. Using these results, cold and hot modal bases are obtained using the POD/MAC procedure. For both cold and hot modes, several basis sets of varying fidelity are examined by comparing the results obtained in physical DoFs with those from the reduced-order analyses.

Once computationally efficient and accurate cold and hot modal bases are established (section *C.1)*, they are utilized for modal basis robustness studies under altered loading conditions as presented in section *C.2*. The altered loading conditions include 0°F/128 dB and 0°F/170 dB cases. Therefore, in both robustness study cases, the ambient temperature is used to evaluate the stiffness and consequently the beam is unbuckled. The 128 dB loading results in a nearly linear response regime, while the 170 dB excitation induces a strongly nonlinear response. The performance of each basis is assessed based on the transverse and in-plane displacement PSD results and is correlated with the modal coupling interactions specific to each basis and with the modal stiffness evaluation conditions. A third basis, consisting of *warm* modes obtained under a heated, but unbuckled condition, is considered to further explain the coupling mechanisms.

Finally, based on the two robustness study cases involving low 128 dB and high 170 dB acoustic loading excitations, section *C.2* discusses the relative importance of linear and nonlinear stiffness components as the response levels change. This study involves again only the cold and hot modal bases.

### *C.1. Eigenanalysis and Modal Basis Selection*

Eigenanalyses of the stress-free ($\Delta T = 0$°F) and thermally pre-stressed beam in the post-buckled regime ($\Delta T = 35$°F) were first performed using ABAQUS Standard. Table 1 presents the low-frequency transverse displacement dominated cold and hot modes and Table 2 presents the high-frequency in-plane displacement dominated cold and hot modes.

The POD/MAC procedure was performed under the most severe loading condition, i.e., 35°F/170 dB. Based on the previous experience with the POD/MAC procedure application,[4] a cumulative POM participation of 99.99% was used to determine the modal basis. This resulted in selection of a stress-free modal basis consisting of 17 cold modes, including 7 transverse modes and 10 in-plane modes. The same procedure utilizing thermally pre-stressed modes resulted in selection of a basis consisting of 17 hot modes, 7 of which were transverse displacement dominated and 10 of which were in-plane displacement dominated. While the number and type of modes identified are the same for the cold and hot modes, the modes themselves are not. The results are summarized in Table 1 and Table 2. It can be observed that the low frequency modes (Table 1) are significantly affected by the thermal loading, as evidenced by the altered ordering of the modes and relative frequency shifts. In contrast, the high-frequency modes (Table 2) and their MAC values are minimally affected by the temperature rise. It is also observed that MAC values associated with the high-frequency modes are generally lower than those obtained for the low-frequency modes. The MAC values for the cold and hot low-frequency modes differ slightly. On average, the cold modes resemble the POMs marginally better than do the hot modes. Finally, for each POM, only a single stress-free

or pre-stressed NM was identified by the MAC, indicating that the POM is not highly distorted under this highly nonlinear response regime. In general, the POD/MAC approach can identify from zero to several NMs bearing resemblance to each POM.

Table 1: POD/MAC results for the low-frequency transverse displacement dominated bases. The POD analysis was performed under the 35°F/170 dB loading condition.

| POM Number | POV (%) | Cumulative POV (%) | Stress-free (Cold) NMs | | | Pre-stressed (Hot) NMs | | |
|---|---|---|---|---|---|---|---|---|
| | | | NM Number | NM Natural Frequency (Hz) | MAC | NM Number | NM Natural Frequency (Hz) | MAC |
| 1 | 85.39 | 85.39 | 1 | 57.817 | 0.998 | 2 | 138.69 | 0.933 |
| 2 | 10.68 | 96.07 | 2 | 159.34 | 0.999 | 1 | 114.47 | 0.998 |
| 3 | 3.10 | 99.17 | 3 | 312.29 | 0.998 | 3 | 327.12 | 0.929 |
| 4 | 0.52 | 99.69 | 4 | 516.05 | 0.999 | 4 | 469.34 | 0.998 |
| 5 | 0.25 | 99.94 | 5 | 770.56 | 1.000 | 5 | 730.86 | 0.995 |
| 6 | 0.03 | 99.97 | 7 | 1431.3 | 1.000 | 7 | 1384.1 | 0.999 |
| 7 | 0.02 | 99.99 | 6 | 1075.7 | 0.999 | 6 | 1027.1 | 0.999 |

Table 2: POD/MAC results for the high-frequency in-plane displacement dominated bases. . The POD analysis was performed under the 35°F/170 dB loading condition.

| POM Number | POV (%) | Cumulative POV (%) | Stress-free (Cold) NMs | | | Pre-stressed (Hot) NMs | | |
|---|---|---|---|---|---|---|---|---|
| | | | NM Number | NM Natural Frequency (Hz) | MAC | NM Number | NM Natural Frequency (Hz) | MAC |
| 1 | 68.99 | 68.99 | 15 | 5,625 | 0.974 | 15 | 5,629 | 0.974 |
| 2 | 18.59 | 87.58 | 22 | 11,250 | 0.962 | 22 | 11,245 | 0.962 |
| 3 | 4.62 | 92.20 | 28 | 16,874 | 0.861 | 28 | 16,861 | 0.861 |
| 4 | 4.51 | 96.71 | 33 | 22,495 | 0.990 | 33 | 22,478 | 0.990 |
| 5 | 1.40 | 98.11 | 38 | 28,114 | 0.721 | 38 | 28,091 | 0.721 |
| 6 | 1.14 | 99.25 | 42 | 33,729 | 0.944 | 42 | 33,701 | 0.944 |
| 7 | 0.38 | 99.63 | 51 | 44,947 | 0.641 | 51 | 44,911 | 0.641 |
| 8 | 0.25 | 99.88 | 47 | 39,340 | 0.930 | 47 | 39,309 | 0.930 |
| 9 | 0.07 | 99.95 | 58 | 56,144 | 0.880 | 58 | 56,096 | 0.880 |
| 10 | 0.04 | 99.99 | 54 | 50,548 | 0.582 | 54 | 50,506 | 0.582 |

Following evaluation of the stiffness at 35°F, the reduced-order simulations for the 35°F/170 dB loading condition were performed using the 17-cold mode and the 17-hot mode bases. Both simulation results compared very favorably with the simulation in physical DoFs. Results at the quarter-span location for the transverse and in-plane displacement components are presented in Figure 2 and Figure 3, respectively.

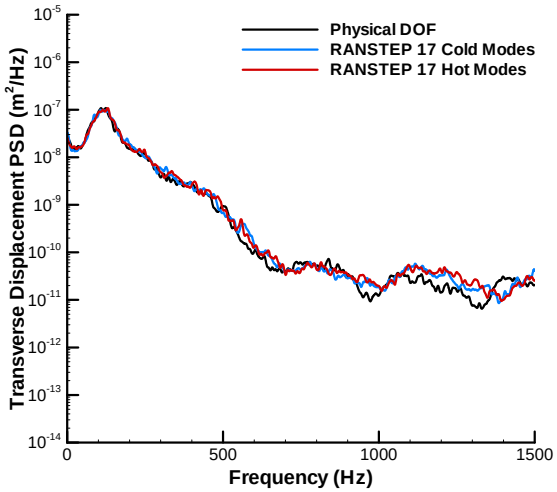


Figure 2: 35°F/170 dB loading condition transverse displacement PSD, 17-mode bases.

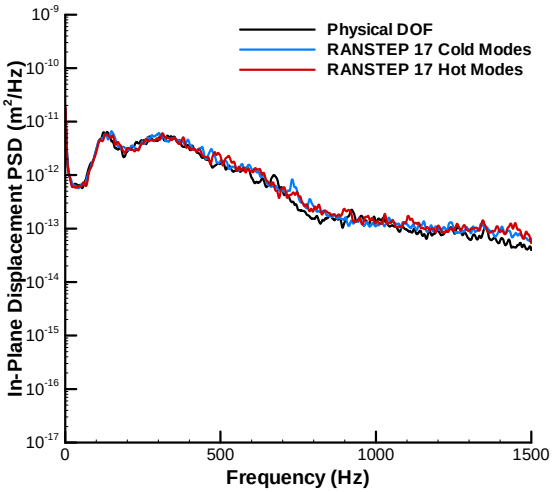


Figure 3: 35°F/170 dB loading condition in-plane displacement PSD, 17-mode bases.

As the reduced-order results presented in Figure 2 and Figure 3 closely resemble the physical DoFs solution, the question becomes whether comparable results can be obtained with a fewer number of modes. If so, does either modal basis more accurately resemble the physical DoF solution than the other in this situation? To investigate this question, the cumulative POM participation factor was reduced from 99.9% to 99.5% and to 95.0%, yielding 11- and 6-mode bases for both classes of modes, respectively. Results for the 6-mode bases (two transverse and four in-plane displacement dominated modes) are presented for the transverse and in-plane displacement components in Figure 4 and Figure 5, respectively. Results for the 11-mode bases (four transverse and seven in-plane displacement dominated modes) are presented for the transverse and in-plane displacement components in Figure 6 and Figure 7, respectively.

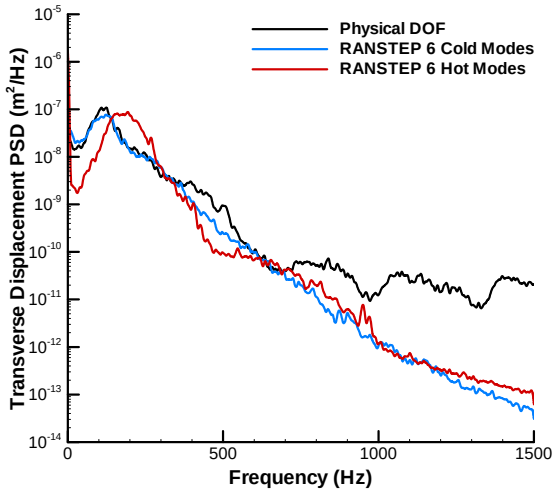


Figure 4: 35°F/170 dB loading condition transverse displacement PSD, 6-mode bases.

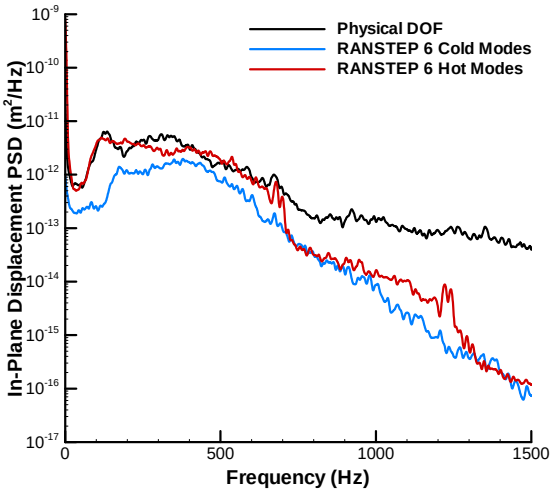


Figure 5: 35°F/170 dB loading condition in-plane displacement PSD, 6-mode bases.

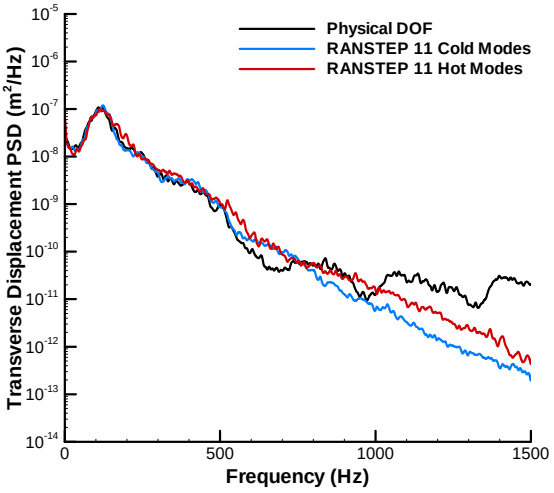


Figure 6: 35°F/170 dB loading condition transverse displacement PSD, 11-mode bases.

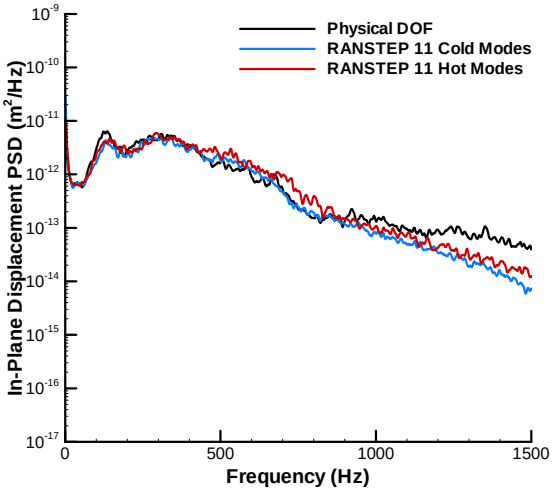


Figure 7: 35°F/170 dB loading condition in-plane displacement PSD, 11-mode bases.

It is seen that the results obtained with the 6-mode bases do not agree well the physical DoF solution. It can be argued that the cold modes perform better when the transverse displacement response is examined, and that the hot modes perform better when the in-plane displacement response is examined. However, the overall conclusion is that both 6-mode bases are insufficient. Results from the 11-mode case further demonstrate that while additional modes improve the comparison of both reduced-order solutions with the physical DoF solution, neither basis is substantially better than the other. In summary, there is no evidence to suggest that a hot mode basis can achieve an accurate solution with fewer modes than a cold mode basis, and vice versa.

*C.2. Modal Basis Robustness Studies and Modal Coupling Investigations*

Next, the modal basis determined through the POD/MAC procedure under the most severe loading conditions of 35°F/170 dB were utilized to simulate the response under a changed loading condition, i.e. 0°F/128 dB. This exercise addresses the range of applicability of each basis. The modal stiffness was re-evaluated under this thermal loading condition, so although the modal bases were the same as in the 35°F case, the stiffnesses were not. The quarter-span transverse and in-plane displacement responses are presented in Figure 8 and Figure 9, respectively.

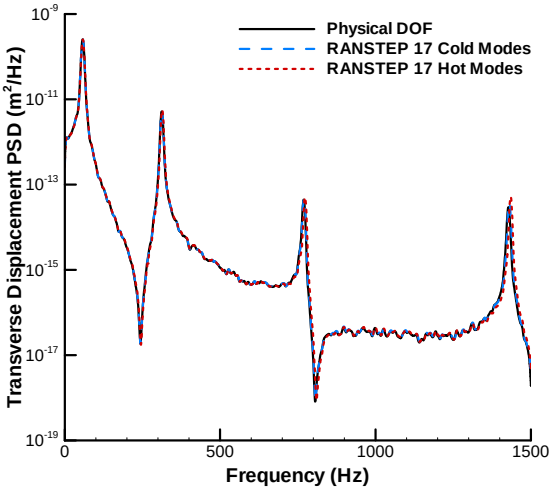


Figure 8: 0°F/128 dB loading condition transverse displacement PSD, 17-mode bases.

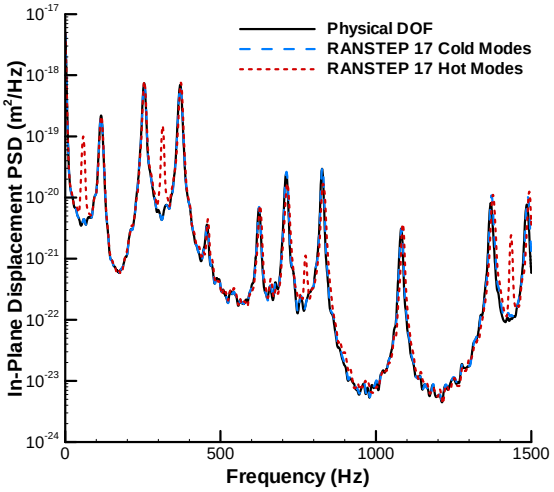


Figure 9: 0°F/128 dB loading condition in-plane displacement PSD, 17-mode bases.

It is seen that the transverse displacement responses obtained with the cold and the hot mode bases resemble the physical DoF simulation response in an almost exact fashion. This is also the case for the in-plane displacement component when the cold modes are used. The simulation utilizing hot modes, however, introduces an erroneous response. It indicates four additional peaks occurring at frequencies nearly identical to the first four symmetric transverse cold modes, i.e., modes 1, 3, 5, and 7 (see Table 1). To explain this behavior, the linear modal stiffness matrices at ambient temperature are presented in Figure 10 and Figure 11 for the cold and hot mode bases, respectively. In both figures, the combined low-frequency transverse modes and high-frequency in-plane modes are arranged in order of increasing frequency from left to right and from top to bottom. For example, the upper left cell in Figure 10 represents the modal stiffness term $d_{1\text{-}1}$ (corresponding to cold mode number 1), and the lower right cell represents the modal stiffness term $d_{54\text{-}54}$ (corresponding to cold mode number 54). Due to modal switching, the upper left cell in Figure 11 represents the modal stiffness term $d_{2\text{-}2}$ (corresponding to hot mode number 2). Figure 10 shows clearly that, as expected, the cold mode linear stiffnesses evaluated at ambient temperature are linearly uncoupled for this planar isotropic structure. On the other hand, Figure 11 shows that the hot mode linear stiffnesses are linearly coupled when evaluated at ambient temperature. In particular, the upper right and lower left quadrants of the linear stiffness matrix couple low-frequency transverse modes with high-frequency in-plane modes, and the lower right quadrant indicates coupling between high-frequency in-plane modes. These couplings are introduced because the hot modes were obtained for a curved post-buckled configuration, which couples the transverse and in-plane displacement components.

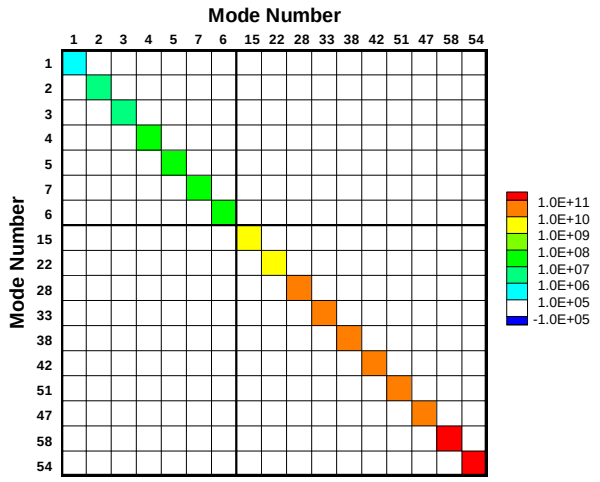


Figure 10: Linear modal stiffness matrix evaluated at the ambient temperature condition with the cold mode basis.

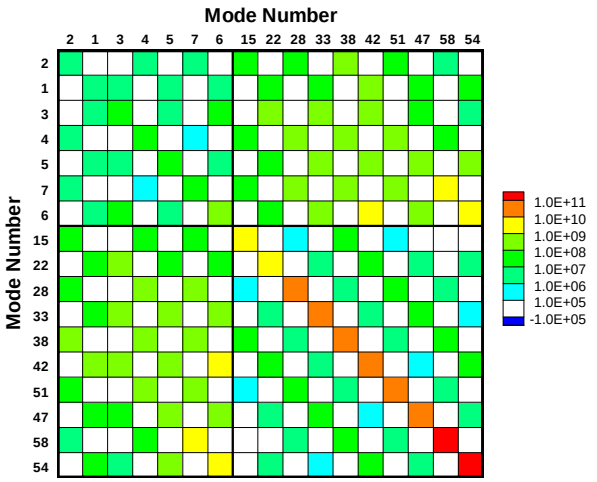


Figure 11: Linear modal stiffness matrix evaluated at the ambient temperature condition with the hot mode basis.

While the use of pre-stressed modes obtained in a thermally *pre-buckled* regime was not the primary focus of this study, consideration of such a case for the 0°F/128 dB loading condition aids in the understanding of the performance of the cold and hot bases. The thermally pre-stressed modes in the pre-buckled regime were obtained at $\Delta T = 2.78$°C (5°F), i.e. $\Delta T = 0.76\,\Delta T_{cr}$. These modes are subsequently referred to as *warm* modes. The process of selecting a warm mode basis was identical to that described for the cold and hot mode bases. The linear modal stiffness matrix evaluated at ambient temperature using the warm mode basis is presented in Figure 12. It is seen that linear coupling exists only between low-frequency transverse modes. Linear coupling does not exist between high-frequency in-plane modes nor, most importantly, between low-frequency transverse and high-frequency in-plane modes. This is because the warm modes, while pre-stressed, are obtained from a flat unbuckled configuration. Consequently, the in-plane displacement PSD obtained with the warm mode basis, presented in Figure 13, shows none of the additional peaks observed for the hot mode basis in Figure 9. More explicitly, the anomalous behavior indicated in Figure 9 is not attributable to coupling between low-frequency transverse modes.

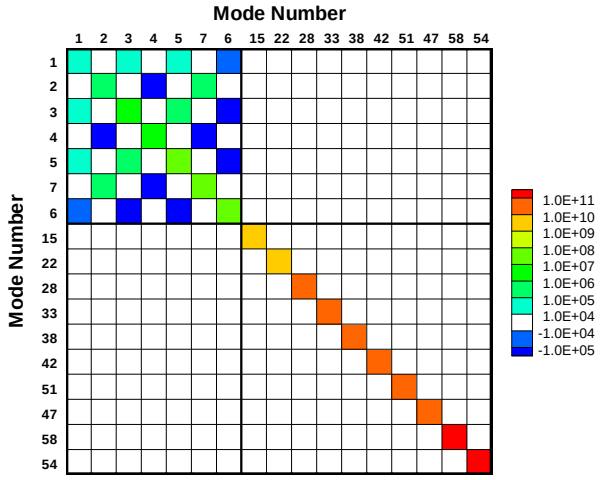


Figure 12: Linear modal stiffness matrix evaluated at the ambient temperature with the warm mode basis.

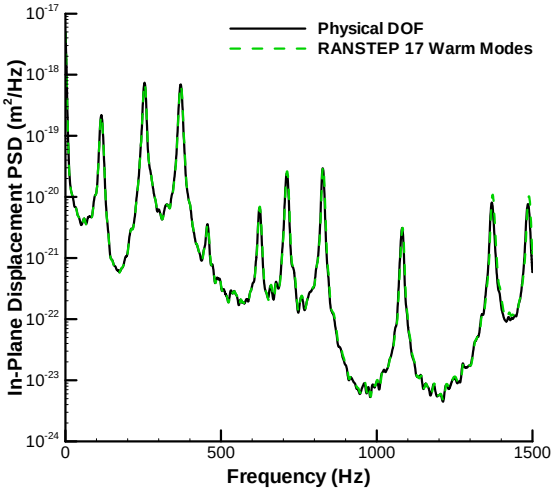


Figure 13: 0°F/128 dB loading condition in-plane displacement PSD, 17-mode warm bases.

To further investigate the effects of coupling, the linear modal stiffness matrices evaluated at the elevated temperature condition are presented in Figure 14 and Figure 15 for the cold and hot mode bases, respectively. It is seen in Figure 14, that the use of cold modes in the thermally post-buckled response analysis introduces linear coupling between low-frequency transverse displacement modes, while coupling between low-frequency transverse displacement modes and high-frequency in-plane displacement modes, and coupling between only high-frequency modes is not present. This further substantiates the finding that coupling between low-frequency transverse modes is not responsible for producing additional peaks in the response PSD. Since the structure is thermally post-buckled, the lowest three diagonal stiffness terms are negative, as shown in Figure 14. As previously demonstrated,[13] the number of negative diagonal stiffness terms increases with increasing temperature above $\Delta T_{cr}$.

The use of hot modes in the thermally post-buckled response analysis, Figure 15, yields a similar coupling distribution to that found in the ambient temperature analysis, see Figure 11. The mechanism through which the coupling is introduced is the same as for the ambient temperature analysis utilizing the hot modes, i.e., the thermally post-buckled deflection. It is also observed that as long as the analysis temperature does not exceed the temperature under which the hot modes were obtained, diagonal stiffness terms will not assume negative values. In the course of previous studies[13] it was concluded that the linear stiffness coefficients obtained with cold modes vary linearly with temperature change. The same observation was made when hot modes were utilized in the present study. The linear variation with temperature change affects both diagonal and off-diagonal terms.

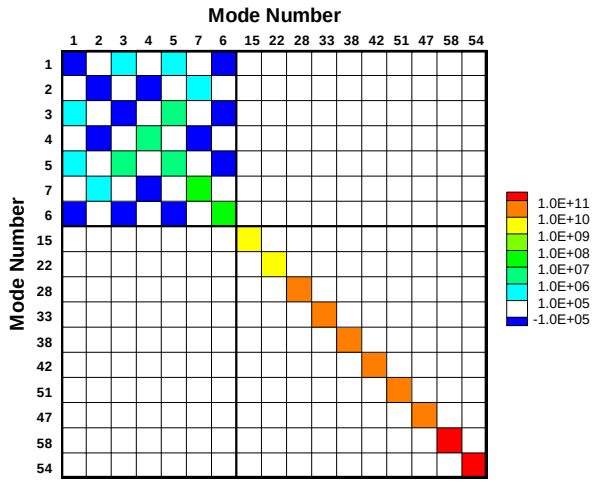


Figure 14: Linear modal stiffness matrix evaluated at the elevated temperature condition with the cold mode basis.

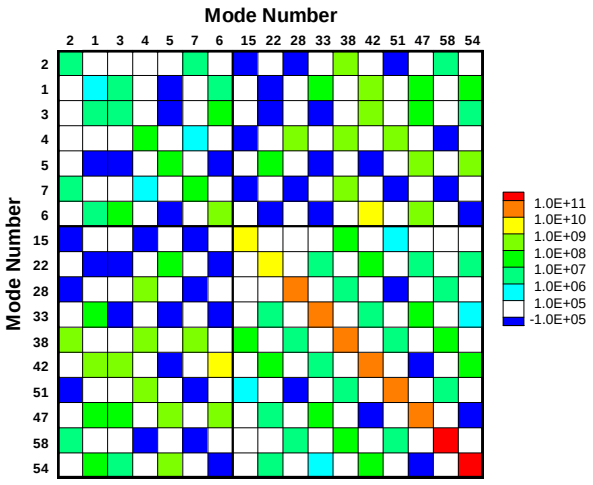


Figure 15: Linear modal stiffness matrix evaluated at the elevated temperature condition with the hot mode basis.

The last case examined herein is intended to provide insight into the relative magnitude of the linear and nonlinear modal coupling in the reduced-order model. Figure 16 and Figure 17 present the quarter-span transverse and in-plane displacement results, respectively, for the 0°F/170 dB load case. Like the nearly linear response PSDs presented in Figure 8 and Figure 9, these results were computed with the stiffness values evaluated at ambient temperature conditions. Since Figure 17 does not indicate the erroneous peak behavior observed in Figure 9, it can be concluded that the significance of linear coupling decreases with increasing nonlinearity. This is because the linear stiffness is independent of the magnitude of the response, and therefore the amount of linear coupling that exists in the 0°F/170 dB case is the same as the amount in the 0°F/128 dB case. At the same time, the amount of nonlinear coupling increases from a negligible amount for the 0°F/128 dB case, to a sizeable amount for the 0°F/170 dB case.

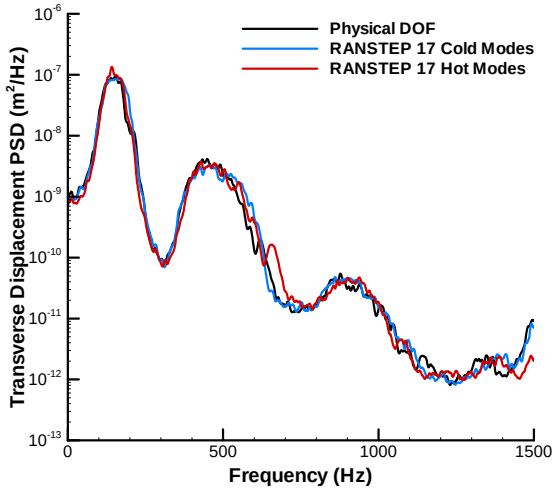


Figure 16: 0°F/170 dB loading condition transverse displacement PSD, 17-mode bases.

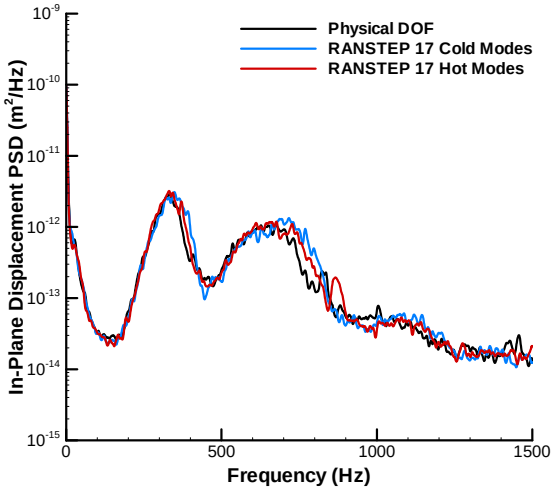


Figure 17: 0°F/170 dB loading condition in-plane displacement PSD, 17-mode bases.

## IV. Conclusions

The merits of applying the stress-free (cold) and thermally pre-stressed (hot) modes in the reduced-order thermal-acoustic response analysis were investigated. The POD/MAC procedure was used to select the modes from both classes of basis functions, thus allowing comparisons to be based on the same modal convergence metric. The reduced-order simulation utilizing the cold mode basis compared favorably with the physical DoFs response over a broad range of loading cases examined. On the other hand, the reduced-order system utilizing the hot mode basis was found to carry a fixed amount of linear coupling due to the post-buckled state under which the eigenanalysis was performed. Consequently, the hot mode basis was found to produce undesirable results when applied to conditions under which this coupling did not exist. The significance of the linear coupling was shown to decrease with increasing nonlinearity. Finally, for the loading cases considered, there were no appreciable differences observed in the modal convergence rates using cold modes versus hot modes.

## References


[1]Blevins, R.D., et al., "Thermo-vibro-acoustic loads and fatigue of hypersonic flight vehicle structure phase II report," ROHR Industries, Inc. RHR 89-202, Chula Vista, CA 1989.

[2]Przekop, A. and Rizzi, S.A., "An efficient modal basis selection criteria for reduced-order nonlinear simulation," *Proceedings of the 7th European Conference on Structural Dynamics EURODYN 2008*, Paper E69, Southampton, UK, 2008.

[3]Przekop, A. and Rizzi, S.A., "Nonlinear reduced-order analysis with time-varying spatial loading distribution," *Proceedings of the 49th AIAA/ASME/ASCE/AHS/ASC Structures, Structural Dynamics and Materials Conference*, AIAA-2008-2323, Schaumburg, IL, 2008.

[4]Rizzi, S.A. and Przekop, A., "System identification-guided basis selection for reduced-order nonlinear response analysis," *Journal of Sound and Vibration*, Vol. 315, No. 3, 2008, pp. 467-485.

[5]Feeny, B.F., "On proper orthogonal co-ordinates as indicators of modal activity," *Journal of Sound and Vibration* Vol. 255, No. 5, 2002, pp. 805-817.

[6]Feeny, B.F. and Kappagantu, R., "On the physical interpretation of proper orthogonal modes in vibrations " *Journal of Sound and Vibration*, Vol. 211, No. 4, 1998, pp. 607-616.

[7]Allemang, R.J. and Brown, D.L., "A correlation coefficient for modal vector analysis," *Proceedings of The 1st International Modal Analysis Conference*, Orlando, FL, 1982, pp. 110-116.

[8]Guo, X. and Mei, C., "Using aeroelastic modes for nonlinear panel flutter at arbitrary supersonic yawed angle," *AIAA Journal*, Vol. 41, No. 2, 2005, pp. 272-279.

[9]Guo, X., Przekop, A., Mei, C., and Lee, Y.Y., "Thermal buckling suppression of supersonic vehicle surface panels using shape memory alloy," *Journal of Aircraft*, Vol. 41, No. 6, 2004, pp. 1498-1504.

[10]Spottswood, S.M., Hollkamp, J.J., and Eason, T.G., "On the use of reduced-order models for a shallow curved beam under combined loading," *Proceedings of the 49th AIAA/ASME/ASCE/AHS/ASC Structures, Structural Dynamics and Materials Conference*, AIAA-2008-2235, Schaumburg, IL, 2008.

[11]Muravyov, A.A. and Rizzi, S.A., "Determination of nonlinear stiffness with application to random vibration of geometrically nonlinear structures," *Computers and Structures*, Vol. 81, No. 15, 2003, pp. 1513-1523.

[12]Rizzi, S.A. and Przekop, A., "Estimation of sonic fatigue by reduced-order finite element based analyses," *Structural Dynamics: Recent Advances, Proceedings of the 9th International Conference*, Southampton, UK, 2006, M.J. Brennan, et al. (ed.).

[13]Przekop, A. and Rizzi, S.A., "Dynamic Snap-Through of Thin-Walled Structures by a Reduced-Order Method," *AIAA Journal*, Vol. 45, No. 10, 2007, pp. 2510-2519.

[14]"ABAQUS version 6.8 On-line Documentation, ABAQUS Analysis User's Manual, Section 6.3.3 " Dassault Systems Simulia Corp., 2008.

[15]"MSC.Nastran 2005 quick reference guide," MacNeal Schwendler Corporation, 2004.

[16]Rizzi, S.A. and Muravyov, A.A., "Comparison of nonlinear random response using equivalent linearization and numerical simulation," *Structural Dynamics: Recent Advances, Proceedings of the 7th International Conference*, Vol. 2, Southampton, UK, 2000, N.S. Ferguson, et al. (ed.), The Institute of Sound and Vibration Research, University of Southampton, pp. 833-846.